Published in final edited form as:
Cell Metab. 2012 November 7; 16(5): 634–644. doi:10.1016/j.cmet.2012.10.006.

Metabolomics identifies an inflammatory cascade involved in dioxin- and diet-induced steatohepatitis

Tsutomu Matsubara[1,4,#], **Naoki Tanaka**[1,#], **Kristopher W. Krausz**[1], **Soumen K. Manna**[1], **Dong Wook Kang**[2], **Erik R. Anderson**[3], **Hans Luecke**[2], **Andrew D. Patterson**[1,5], **Yatrik M. Shah**[3], and **Frank J. Gonzalez**[1,*]

[1]Laboratory of Metabolism, Center for Cancer Research, National Cancer Institute, National Institutes of Health, Bethesda, MD 20892

[2]Laboratory of Bioorganic Chemistry, National Institute of Diabetics and Digestive and Kidney Diseases, National Institutes of Health, Bethesda, MD 20892

[3]Department of Molecular and Integrative Physiology and Internal Medicine, Division of Gastroenterology, University of Michigan School of Medicine, Ann Arbor, MI 48109

Summary

2,3,7,8-Tetrachlorodibenzo-p-dioxin (TCDD) is among the most potent environmentally toxic compounds. Serum metabolomics identified azelaic acid-mono esters as significantly increased metabolites after TCDD treatment, due to down-regulation of hepatic carboxylesterase 3 (CES3, also known as triglyceride hydrolase) expression in an arylhydrocarbon receptor (AhR)-dependent manner in mice. The decreased CES3 expression was accomplished by TCDD-stimulated TGFβ-SMAD3 and IL6-STAT3 signaling, but not by direct AhR signaling. Methionine- and choline-deficient (MCD) diet-treated mice also showed enhanced serum azelaic acid-mono ester levels following attenuation of hepatic CES3 expression, while *db/db* mice did not, thus suggesting an association with steatohepatitis. Forced expression of CES3 reversed serum azelaic acid-mono ester/azelaic acid ratios and hepatic TGFβ mRNA levels in TCDD- and MCD diet-treated mice and ameliorated steatohepatitis induced by MCD diet. These results support the view that azelaic acid-mono esters are possible indicators of TCDD exposure and steatohepatitis, and suggest a link between CES3, TGFβ, and steatohepatitis.

Introduction

A number of chemical contaminants highly prevalent in the environment elicit some or all of their toxicity through the arylhydrocarbon receptor (AhR), a ligand-activated transcription factor. Activated AhR forms a heterodimer together with the AhR nuclear translocator (ARNT) and binds to xenobiotic response elements in the promoter regions of target resulting in induction or inhibition of expression. Among the AhR target genes are the cytochrome P450 (CYP) 1A1, CYP1A2 and CYP1B1 (Nebert et al., 2004). Many polycyclic

*Correspondence: Frank J. Gonzalez, Laboratory of Metabolism, National Cancer Institute, Building 37, Room 3106, Bethesda, MD 20892, Tel: 301-402-9067, Fax: 301-496-8419, gonzalef@mail.nih.gov.
[4]Current address; Department of Anatomy and Regenerative Biology, Osaka City University, Osaka, Japan
[5]Current address; Center for Molecular Toxicology and Carcinogenesis, Department of Veterinary and Biomedical Sciences, The Pennsylvania State University, University Park, PA 16802
#The authors equally contributed to this work.

aromatic hydrocarbons and polychlorinated biphenyls are activators of AhR/ARNT signaling and considered carcinogenic either individually or as part of mixtures. 2,3,7,8-Tetrachlorodibenzo-p-dioxin (TCDD) is among the most notorious; accidental exposure of humans to TCDD is associated with birth defects, increased risk of cancer and the development of chronic disease in exposed individuals. In animal studies, TCDD exposure leads to a variety of toxicities in the immune system and liver, and birth defects when administered during pregnancy (Rifkind, 2006). The mechanisms of how TCDD induces toxicities have been investigated in mouse models, notably the *Ahr*-null ($Ahr^{-/-}$) mouse is resistant to thymus atrophy, hepatomegaly, pulmonary lesion, immunotoxicity, and teratogenesis (Fernandez-Salguero et al., 1995; Fernandez-Salguero et al., 1996; Peters et al., 1999; Thomae et al., 2004; Thurmond et al., 2000; Vorderstrasse et al., 2001).

To develop a better understanding of the biochemical events underlying TCDD toxicity, global gene expression was investigated by microarray analysis (Fletcher et al., 2005; Hanlon et al., 2005). Another approach to unravel the mechanism of toxicity is to determine the effect of TCDD on serum and urine metabolites. Metabolomics, based on ultra-performance liquid chromatography coupled with electrospray ionization quadrupole time-of-flight mass spectrometry (UPLC-ESI-QTOFMS), is a potent tool for the detection and characterization of small organic chemicals in biological matrices (Idle and Gonzalez, 2007; Johnson et al., 2011). Recently, TCDD-induced changes in serum metabolites were analyzed and TCDD exposure was reported to enhance serum lysophosphatidylcholine (22:5) and lysophosphatidylethanolamine (18:1, 18:2 and 18:3) and attenuate serum fatty acids (eicosapentaenoic acid and docosahexaenoic acid) (Lin et al., 2011). However, it was unclear whether these metabolites were involved in TCDD toxicity.

In the current study, dose- and time-dependent changes in serum metabolites after TCDD exposure were investigated with UPLC-ESI-QTOFMS. In addition, mouse models of Ahr/ARNT signaling were used to clarify the mechanism. These combinational analyses provided early biomarkers associated with the TCDD-induced liver injury furthering the understanding of the molecular mechanism.

Results

TCDD exposure altered serum azelaic acid metabolites depending on hepatic AhR/ARNT signal

The influence of TCDD exposure on serum metabolites was investigated in male mice administered TCDD (10 or 200 μg/kg body weight) or vehicle (10% DMSO/90% corn oil). Low-dose TCDD (10 μg/kg) did not significantly change serum alanine and aspartate aminotransferase (ALT and AST, respectively) activities while high-dose TCDD (200 μg/kg) increased both markers for hepatotoxicity (Figures S1A and S1B). Hepatic injury was observed only at high-dose TCDD (Figure S1C). Induction of hepatic CYP1A1 and CYP1A2 expression, prototypical AhR target genes, was found with both low- and high-dose TCDD (Figure S1D). Partial least squares-discriminant analysis (PLS-DA) on UPLC-ESI-QTOFMS negative mode data from serum of mice exposed to 200 μg/kg of TCDD revealed separation between the control and TCDD groups (Figure 1A) that was further examined in the loading plot (Figure 1B). PLS-DA with UPLC-ESI-QTOFMS positive mode data also showed clear separation between the groups (data not shown). The contribution analysis indicated 20 ions as the top-ranking ions giving rise to the separation in negative and positive modes (Tables S2 and S3). The most attenuated ion was metabolite 0 (M0, $m/z = 187.0968^-$ at 2.12 min). In the enhanced ions group, the top 2 ions were metabolite 1 (M1, $m/z = 273.1684^-$ at 3.02 min) and metabolite 2 (M2, $m/z = 245.1380^-$ at 2.48 min). The decrease in serum M0 levels and the increase in serum M1 and M2 levels were time-dependent after TCDD injection (Figure 1C). The identification was performed

by tandem mass spectrometry MS/MS fragmentation with authentic chemicals. The MS/MS fragmentation of M0 showed $m/z = 97^-$, 125^- and 187^-, and the fragmentation pattern was the same as that of authentic azelaic acid (Figure S2A, left). Thus, M0 was determined as azelaic acid (Az) (Figure 1D). The MS/MS fragmentation of M2 showed $m/z = 97^-$, 125^-, 187^-, and 245^- (Figure S2A, middle) and was identified as azelaic acid-mono-hydroxy-propyl ester. In addition, M2 was determined to be a mixture of 3 structural isomers, nonanedioic acid mono-(3-hydroxy-propyl) ester (M2a), nonanedioic acid mono-(2-hydroxy-propyl) ester (M2b), and nonanedioic acid mono-(2-hydroxy-1-methyl-ethyl) ester (M2c), using an optimized UPLC-ESI-TOFMS (Figures 1D and S2B). The MS/MS fragmentation of M1 showed $m/z = 97^-$, 125^-, 187^-, and 273^- (Figure S2A, right) and M1 was expected as azelaic acid-mono-hydroxy-pentyl ester. The MS/MS fragmentation pattern of the authentic chemical was the same as that of M1, but the retention time differed from that of M1 (data not shown). M1 was not identified, although it was expected as Az ester (structure presented in Figures S2D and S2E). Serum Az and M2 levels were measured in C57BL/6 mice 7 days after TCDD injection. TCDD exposure decreased the Az levels [Oil, TCDD(+) and TCDD(++) was 43.8 ± 9.9, 28.3 ± 4.8, and 26.2 ± 0.8 μM, respectively] and increased the M2 levels [Oil, TCDD(+) and TCDD(++) was 1.8 ± 1.7, 6.9 ± 3.1 and 8.8 ± 1.7 μM, respectively] in a dose-dependent manner (Figure 1E). To determine whether the alterations in serum metabolites were dependent on AhR/ARNT signaling, TCDD was administered to $Ahr^{-/-}$, hepatocyte-specific *Arnt*-null ($Arnt^{\Delta Liv}$), and intestinal epithelial cell-specific *Arnt*-null ($Arnt^{\Delta IE}$) mice. Metabolomic analysis demonstrated that serum metabolite changes associated with TCDD treatment in wild-type littermate mice were not observed in the $Ahr^{-/-}$ and $Arnt^{\Delta Liv}$, but were similar to wild-type mice in the $Arnt^{\Delta IE}$ mice (Figure S3A). The TCDD-stimulated increase in M2 levels was attenuated in the $Ahr^{-/-}$ and $Arnt^{\Delta Liv}$ mice, but not in the $Arnt^{\Delta IE}$ mice (Figure 1F). Moreover, the TCDD-stimulated changes in serum ALT activities and Az and M1 levels were not found in the $Ahr^{-/-}$ and $Arnt^{\Delta Liv}$ mice, while the changes in the $Arnt^{\Delta IE}$ mice were similar to the $Arnt^{F/F}$ mice (Figures S3B–D). These results suggest that TCDD exposure alters serum metabolites through hepatic AhR/ARNT signaling and is associated with liver injury.

TCDD exposure lowered hepatic hydrolase activity to M2 following attenuation of hepatic carboxylesterase 3 expression in AhR/ARNT-dependent manner

Kinetic analysis of M2 metabolism in the C57BL/6 mouse was performed revealing maximum enzyme velocity (Vmax) values of M2a, M2b and M2c of 47.0, 42.5 and 38.0 nmol/min/mg microsomal protein, respectively (Figures 2A–C). The Michaelis-Menten constant (Km) of M2a, M2b and M2c were 79.5, 71.2 and 96.1 μM, respectively. Furthermore, the metabolic activities were attenuated in a hepatic AhR/ARNT-dependent manner (Figures 2D–F). These results suggest that TCDD-induced attenuation of hepatic hydrolase activity enhances serum M2 levels. Levels of mRNAs encoding carboxylesterases (CES) 1 to 6 were measured to determine which CES was involved in the M2 metabolism. CES3 [also known as triglyceride hydrolase (TGH) and CES1D] mRNA levels were decreased in a dose-dependent and time-dependent manner after TCDD exposure while CES6 (also known as CES2A) mRNA slightly decreased (Figure 3A). The attenuation of CES3 expression was dependent on hepatic AhR/ARNT expression, while that of the CES6 expression was not, although the changes were lower in $Ahr^{-/-}$ mice (Figures 3B and 3C). In addition, non-denaturing gel electrophoresis indicated that TCDD lowered hepatic CES3 protein and activity levels in hepatic AhR/ARNT-dependent manner (Figures 3D–F). Furthermore, overexpression of CES3 in HEK293 cells enhanced the M2 metabolic activity while CES6 did not (Figure 3G). These results suggest that CES3 catalyzes the M2 hydrolytic reaction and is a key factor for TCDD-induced alterations of serum metabolites.

TCDD suppressed hepatic CES3 expression via activation of TGFβ-SMAD3 and IL6-STAT3 signals

Decreased CES3 expression was not observed in primary hepatocytes after 20 nM of TCDD exposure, although the hepatocytes showed induction of CYP1A2 expression (Figure 4A), indicating that the Ahr signaling pathway was intact. Pro-inflammatory cytokines are known to regulate gene expression in liver. TCDD-induced expression of the mRNAs encoding tumor necrosis factor α (TNFα), interleukin (IL) 6, and transforming growth factor β (TGFβ) in liver was found in an AhR/ARNT-dependent manner (Figures 4B–D); the mRNA encoding IL1β was not induced in TCDD-treated *Arnt*$^{F/F}$ mice. In addition, the induction was also observed 3 days after TCDD injection (data not shown). TCDD-exposed liver showed a significant increase of IL6 and active TGFβ proteins and a slight increase of TNFα protein (Table S4). Thus, the influence of TNFα, IL6 and TGFβ on hepatic CES3 expression was investigated with primary hepatocytes. Both IL6 (100 ng/mL) and TGFβ (10 ng/mL) exposure decreased the CES3 mRNA levels and TNFα (100 ng/mL) exposure increased expression, under conditions where expression of bonafide target genes [suppressor of cytokine signaling 3 (SOCS3) for IL6, nitric oxide synthase 2 (iNOS) for TNFα, and collagen type I α 1 (COL1A1) for TGFβ, respectively] were induced (Figure 4E). Luciferase reporter assays suggested that the *Ces3* gene promoter region (−1398 to −699) had a negative regulatory element since constitutive luciferase activity of the *Ces3*-1.4k reporter is lower than that of *Ces3*-0.7k reporter (Figure S4A). Both IL6 and TGFβ exposure attenuated luciferase activity of the *Ces3*-1.4k reporter with putative signal transducer and activator of transcription 3 (STAT3)- and MAD homolog 3 (SMAD3)-binding sites in Hepa1c1 cells, but they did not affect the *Ces3*-0.7k reporter without the sites (Figure 4F). In addition, introduction of STAT3 or SMAD3 also attenuated the activity of the *Ces3*-1.4k reporter, but not that of the *Ces3*-0.7k reporter (Figures S4B and S4C). Attenuation of this construct by IL6 or TGFβ was diminished by mutation of the STAT3- and/or SMAD3-binding sites (Figure 4F). Co-treatment with IL6 (50 ng/mL) and TGFβ (5 ng/mL) markedly decreased CES3 mRNA levels in primary hepatocytes, compared to the IL6 or TGFβ alone (Figure 4G). Furthermore, *in vivo* chromatin immunoprecipitation (ChIP) assays indicated SMAD3- and STAT3-binding to the *Ces3* gene promoter region after TCDD administration (Figure 4H). These results suggest that TCDD-activated IL6 and TGFβ signaling attenuates CES3 expression in the liver. The effect of IL6 and TGFβ in *Ahr*$^{-/-}$ hepatocyte cultures was not investigated. However, TCDD exposure decreased hepatic CCAAT/enhancer binding protein α (CEBPα) expression, which controls *Ces3* gene expression, in an AhR/ARNT-dependent manner (Figures S4D and S4E). Interestingly, TGFβ attenuated hepatocyte CEBPα expression (Figure S4F), which up-regulates the *Ces3* gene promoter (Figure S4G); IL6 did not alter levels of CEBPα. Thus, TGFβ also decreased hepatic CES3 levels indirectly through attenuation of CEBPα expression.

TCDD elevated hepatic H_2O_2 through induction of xanthine dehydrogenase and NADPH oxidase 2 in an AhR/ARNT-dependent manner

Hepatic H_2O_2 levels were measured to investigate the mechanism by which TCDD stimulates pro-inflammatory cytokine activation. The TCDD-enhanced hepatic H_2O_2 levels were dose- and AhR/ARNT-dependent (Figure S5A). The mRNAs encoding xanthine dehydrogenase (XDH, also known as xanthine oxidase) and NOX2 (NADPH oxidase 2, also known as cytochrome b245-β), the major sources of oxidative stress, were measured in livers. The induction of these genes by TCDD was dose-dependent and was clearly observed at 3 days and 7 days after TCDD administration (Figure S5B); the induction of XDH and NOX2 expression was also AhR/ARNT-dependent (Figures S5C and S5D). Furthermore, TCDD exposure induced XDH and NOX2 in primary hepatocytes (Figure S5E). These results support the view that TCDD directly induces XDH and NOX2 expression via AhR/ARNT signaling and enhances oxidative stress in the liver.

Changes in serum Az metabolites and the related hepatic gene expression are associated with steatohepatitis

TCDD is known to increase hepatic triglyceride (TG) levels. Indeed, TCDD increased the hepatic TG levels in a dose-dependent [Oil, TCDD(+) and TCDD(++) was 9.2 ± 0.8, 36.2 ± 7.8 and 73.0 ± 11.0 μg/mg liver, respectively] and AhR/ARNT-dependent manner (Figure 5A). Serum TG and free fatty acids were not changed in an AhR/ARNT-dependent manner (Table S5). In view of this result, a possible relationship between the serum TCDD marker M2 and fatty liver was investigated using 2 fatty liver animal models, *db/db* mice and methionine- and choline-deficient (MCD) diet-fed mice. Hepatic TG levels were elevated in both mouse models compared to the controls (Figure 5B). The serum M2 levels were enhanced in the MCD diet-treated mice, but not in the *db/db* mice (Figure 5C). A similar phenomenon was also observed with M1 levels (data not shown). The CES3 mRNA expression was attenuated in the MCD diet-treated mice with steatohepatitis, but not in the *db/db* mice with simple steatosis (Figures 5D and 5E). In addition, induction of XDH, NOX2, and TGFβ expression was only observed in the MCD steatohepatitis model (Figures 5D and 5E). TCDD-, AhR/ARNT- and MCD diet-dependent changes in hepatic expression of other TG-related genes were not observed (Figure S6). MCD diet also resulted in a three-fold induction of CYP1A1 mRNA suggesting a small amount of AhR/ARNT signaling activation in the livers of these mice, considerably less than the massive activation of AhR/ARNT signaling seen in TCDD-treated mice (data not shown). These results indicate the importance of hepatic CES3 expression in Az-mono ester metabolism and suggest that the metabolic alterations are related to induction of XDH, NOX2, and TGFβ expression in livers with steatohepatitis.

Hepatic CES3 overexpression attenuated serum M2/Az ratios

To investigate whether CES3 catalyzes M2 hydrolytic reaction *in vivo*, a recombinant adenovirus expressing mouse CES3 was generated (Figure S7A). The adenovirus (2×10^9 pfu/mouse) produced robust expression of CES3 in the liver without increased serum ALT levels 4 days after injection (Figures S7B and S7C). Adenovirus was injected 4 days before the mouse were killed (Figures S7D and S7E) and enhanced both hepatic CES3 mRNA and protein expression (Figures 6A–D) and decreased serum M2/Az ratios (Figures 6E and 6F) in TCDD- and MCD-induced liver injury, although the ratio was not significantly decreased in methionine- and choline-supplemented (MCS) control diet-treated mice (Figure 6F). In addition, with and without CES3 overexpression, hepatic CES3 mRNA levels were negatively correlated with serum M2/Az ratios (Figures 6G and 6H). These results strongly suggest hepatic CES3 mediates M2 hydrolysis *in vivo*. Interestingly, the forced expression of CES3 attenuated the increase in serum ALT levels after MCD treatment, but not after TCDD exposure (Figures 6I and 6J). Furthermore, liver histology revealed that CES3 overexpression alleviated both TCDD- and MCD-induced steatohepatitis (Figures 6K and 6L) and decreased the enhanced hepatic TGFβ mRNA levels (Figures S7F and S7G). This observation may suggest a link between CES3, TGFβ, and steatohepatitis.

Discussion

The current study demonstrated that TCDD increased serum Az-mono ester levels following pro-inflammatory cytokine-induced changes in expression of hepatic CES3 (Figure 7). To further determine the global changes in serum metabolites after TCDD administration, the serum metabolome of the TCDD-exposed mice was interrogated and compared with that of the controls. UPLC-ESI-TOFMS, in conjunction with a PLS-DA, revealed changes in serum metabolites after TCDD exposure, and determined that Az was attenuated while Az-mono esters (M1 and M2) were elevated. Levels of the M1 and M2 in serum were increased in a time-dependent manner after TCDD exposure, even with low-dose (10 μg/kg) TCDD,

which did not significantly increase serum ALT and AST levels. These results suggest that Az-mono esters are early indicators of dioxin exposure.

TCDD affects a variety of organs (Rifkind, 2006). The changes of serum metabolites were diminished in $Arnt^{\Delta Liv}$ mice, but not in $Arnt^{\Delta IE}$ mice, indicating that the TCDD-mediated metabolic alterations were related to hepatic AhR/ARNT signal transduction. Liver microsomes demonstrated hydrolysis of Az-mono esters and showed decreased activity in an AhR/ARNT-dependent manner after TCDD injection. These results indicate that attenuation of hepatic hydrolase activity is correlated with increased Az-mono esters in serum. The hydrolytic enzyme, carboxylesterase, was considered a candidate enzyme catalyzing the hydrolysis of Az-mono esters. Among several forms expressed in mice, CES3 (also called TGH) expression was decreased in a hepatic AhR/ARNT-dependent manner and overexpression of CES3 in HEK293 cells catalyzed hydrolysis of Az-mono esters in microsomes. In addition, forced expression of CES3 in the liver attenuated the TCDD-induced serum ratios of M2 to Az. Furthermore, the ratios showed a negative correlation with the CES3 mRNA levels. Thus, a major reason for the TCDD-mediated increase in serum Az-mono ester levels is likely due to decreased hepatic CES3/TGH expression.

TCDD exposure generates inflammation in the liver (Lu et al., 2011; Shen et al., 1991) and TCDD-induced liver injury is dependent on AhR/ARNT signaling. Hepatocyte AhR/ARNT activation can trigger liver injury and alter serum Az-mono ester levels in mice. TCDD exposure did not lower CES3 expression in primary hepatocytes, thus indicating that the effect is indirect. However, it was previously reported that TCDD can induce expression of XDH and NOX2 in primary hepatocytes in an AhR/ARNT-dependent manner (Sugihara et al., 2001). TCDD also raised H_2O_2 levels in the liver where XDH and NOX2 expression were induced. XDH and NOX2 are known to generate reactive oxygen species (ROS) (Kale, 2003; Lam et al., 2010), such as H_2O_2, and then ROS can in turn stimulate pro-inflammatory cytokine activation (Jaeschke, 2011). Induction of IL6 and TGFβ expression was also dependent on AhR/ARNT in the liver. Furthermore, IL6 and TGFβ decreased CES3 expression through STAT3 and SMAD3 signaling, respectively. Co-treatment with IL6 and TGFβ resulted in a marked attenuation of CES3 expression in hepatocytes, suggesting an interaction between IL6 and TGFβ, as previously reported (Yamamoto et al., 2001). Induction of TNFα mRNA expression was also observed in the liver. However, different from IL6 and TGFβ, TNFα protein was not significantly increased in the liver. The slight enhancement of TNFα protein, which can induce CES3 expression in hepatocytes, may not affect CES3 expression. Additionally, H_2O_2 (400 μM for 6 hours)-induced CES3 suppression was not observed in primary hepatocytes (data not shown). These results strongly support the view that AhR/ARNT activation by TCDD leads to attenuation of CES3 expression in the liver through XDH/NOX2-ROS-cytokine signaling.

Simple steatosis is different from steatohepatitis in pro-inflammatory cytokine activation (Tanaka et al., 2012). MCD diet-fed mice [nonalcoholic steatohepatitis (NASH) model] showed similar alterations in serum Az-mono esters and hepatic gene expression profiles to the TCDD-exposed mice, but *db/db* mice with simple steatosis did not. TCDD is also known to lead to steatohepatitis (Lu et al., 2011) and showed pro-inflammatory cytokine activation in the present study. Among these cytokines, the TCDD-induced TGFβ mRNA levels were highly correlated with serum Az-mono ester levels and hepatic CES3, NOX2, and XDH mRNA levels. In addition, induction of TGFβ expression was observed in the MCD diet-treated mice with elevated serum Az-mono esters following increased hepatic XDH and NOX2 mRNA levels and decreased hepatic CES3 mRNA levels; elevated IL6 expression was not observed. Furthermore, forced expression of CES3 in the liver attenuated the increase in serum ALT levels and hepatic TGFβ mRNA levels and alleviated NASH induced by MCD diet. Although further studies are required to determine how TGFβ

contributes to steatohepatitis, decreased hepatic CES3 activity might reflect TGFβ activation under hepatic inflammation. The TGFβ-mediated decrease in hepatic CES3 activation can mainly cause an elevation of serum Az-mono esters.

This study demonstrated that decreased CES3 expression by TCDD exposure was due to increased pro-inflammatory cytokine signaling. Lower CES3 expression was also associated with steatohepatitis. CES3 expression can be detected by monitoring its metabolism *in vivo* as demonstrated with the altered levels of Az-mono esters. This could lead to a diagnostic test for early signs of dioxin toxicity and steatohepatitis that appear before the onset of liver damage as revealed by increase serum AST and ALT levels.

Experimental Procedures

Materials

Nonane acid mono-(3-hydroxy-propyl) ester, nonanedioic acid mono-(2-hydroxy-propyl) ester, and nonanedioic acid mono-(2-hydroxy-1-methyl-ethyl) ester were synthesized as described in Supplementary materials. TNFα and IL6 were purchased from Sigma-Aldrich (St. Louis, MO) and TGFβ was from R&D systems® (Minneapolis, MA).

Cell culture

HEK293 and COS-1 cells were grown at 37 °C with 5% CO_2 in RPMI 1640 and DMEM (Invitrogen, Grand Island, NY) supplemented with 10% fetal bovine serum (Gemini Bio-Products, Woodland, CA), respectively. To gain CES3- and CES6-overexpressing cells, HEK293 and COS-1 cells were transfected by Fugene 6 (Invitrogen) with CES3- and CES6-expression vector (Origene Technology, Rockville, MD).

Animals and diets

Ahr$^{-/-}$ (Fernandez-Salguero et al., 1995), *Arnt*$^{F/F}$ (Tomita et al., 2000), *Arnt*$^{\Delta Liv}$ (Shah et al., 2009), and *Arnt*$^{\Delta IE}$ (Ito et al., 2007) mice were previously described. C57BL/6NCr and *db/db* mice were purchased from The Jackson laboratories (Bar harbor, ME). Mice were housed in temperature- and light-controlled rooms and were given water and pelleted NIH-31 chow *ad libitum*. In the TCDD studies, mice (7 to 9 weeks old) were injected intraperitoneally with TCDD solution (10% dimethylsulfoxide (DMSO)/corn oil as vehicle). MCD and the control MCS diet (Tanaka et al., 2012) were purchased from Dyets Inc. (Bethlehem, PA) and given to C57BL/6NCr mice (7 to 9 weeks old) for 4 weeks *ad libitum*. *db/db* and the control C57BL/6NCr mice were sacrificed at the age of 12 to 16 weeks. All animal studies were carried out in accordance with Institute of Laboratory Animal Resources (ILAR) guidelines and approved by the National Cancer Institute Animal Care and Use Committee.

Chemical detection and quantification

Serum was prepared using Serum Separator Tubes (Becton, Deckinson and Company, Flanklin lakes, NJ). The serum was diluted with 9 volumes of 66% acetonitrile and centrifuged twice at 18,000*g* for 20 min to remove insoluble materials. UPLC-ESI-QTOFMS analysis was preformed as previously reported (Matsubara et al., 2011). The eluant was introduced by electrospray ionization into the mass spectrometer [Q-TOF Premier® (Waters Corp, Milford, MA)] operating in either negative or positive electrospray ionization modes. To quantify the levels of Az and its mono esters, an Acquity UPLC system coupled with a XEVO triple-quadrupole tandem mass spectrometer (Waters Corp.) was used. Purified standard of each compound was used for quantitation. Multiple reaction monitoring (MRM) was employed and the following MRM transitions were used: 187→125 (Az), 245→125 (metabolite M2a), 245→187 (metabolite M2c), and 275→190

(Chlorpropamide, internal standard). An Acquity UPLC BEH C18 column (1.7 μm, 2.1×150 mm, Waters Corp.) was used to separate the samples. The mobile phase was comprised of 0.1% aqueous formic acid (A) and acetonitrile containing 0.1% formic acid (B). The initial gradient of 2% B was held for 1.5 min, then linearly increased to 60% B at 12 min, and then to 99% B at 18 min. The gradient was held at 99% B for 1 min, and then returned to initial conditions for 2 min for column equilibration. Flow rate was maintained at 0.3 mL/min and column temperature was maintained at 50 °C throughout the run.

Data processing and multivariate data analysis

Data processing and multivariate data analysis were conducted as previously reported (Matsubara et al., 2011). A PLS-DA, PCA, and contribution analyses were performed using SIMCA-P+12 (Umetrics, Kinnelon, NJ).

RNA analysis [quantitative polymerase chain reaction (qPCR) analysis]

RNA was extracted using TRIzol reagent (Invitrogen). qPCR was performed using cDNA generated from 1 μg total RNA with SuperScript II Reverse Transcriptase kit (Invitrogen). Primers were designed using qPrimerDepot. All sequences are listed in Table S1. qPCR reactions were carried out using SYBR green PCR master mix (Applied Biosystems, Foster City, CA) in an ABI Prism 7900HT Sequence Detection System. Values were quantified using the comparative CT method and normalized to 18S ribosomal RNA.

Detection of carboxylesterase in microsomal fractions

Liver was homogenized using 100 mM Tris-HCl (pH 7.5) with a protease inhibitor cocktail (Roche Diagnostics, Indianapolis, IN) for microsomal fractions. The homogenate was centrifuged at 9,000*g*, and then the supernatant was centrifuged at 105,000*g*. The pellet was suspended with 10% Glycerol/100 mM Tris-HCl (pH 7.5). Protein was quantified using the BCA™ Protein Assay Kit (Termo, Rockford, IL). Microsomal proteins were separated with non-denaturing gel electrophoresis and carboxylesterases detected with Fast Blue RR and 1-naphthyl acetate, as previously described (Yang et al., 2001). Briefly, 10 μg of microsomal protein was subjected to non-denaturing gel electrophoresis (7.5% acrylamide gel). The gel was washed for 30 min in 100 mM potassium phosphate buffer (pH 6.5), followed by incubation in the buffer with 1-naphthylacetate (5 mM) and diazotized Fast Blue RR. Esterase staining is based on a black and insoluble complex between the Fast Blue RR and 1-naphtol hydrolyzed from 1-naphthylacetate.

Determination of hydrolase activity to M2

Hepatic microsomal protein (2 μg) was mixed with 50 μL of 100 mM Tris-HCl buffer (pH 7.4) including M2 as substrate (triplicate for each concentration), and incubated at 37°C for 10 min. One-hundred μL of 66% acetonitrile with 4-chloropropamide (internal standard) was added to stop the reaction and extract the metabolites. After vortexing for 1 min, the solution was centrifuged at 18,000*g* for 20 min. The supernatant was subjected to UPLC-ESI-TOFMS to detect the metabolites. The Vmax and Km were determined using Prism® version 5.0c (GraphPad Software Inc., San Diego, CA). HEK293 cells expressing recombinant CES3 and CES6 were cultured in RPMI 1640 with M2 as substrate for 24 hr. The medium was collected and 75% acetonitrile with 4-chloropropamide (internal standard) was added to extract the metabolites. After vortexing for 1 min, the solution was centrifuged at 18,000*g* for 20 min. The supernatant was subjected to the Xevo system to measure the metabolites. The hydrolase activity to M2 was determined as production of the product Az from M2.

Preparation and culture of hepatocytes

Hepatocytes were prepared by general perfusion method with 2 mg/mL collagenase (Matsubara et al., 2011). The viability of isolated hepatocytes was checked with trypan blue dye exclusion and those with higher than 85% viability were used. The hepatocyte was incubated at 37°C with 5% CO_2 in DMEM with 1% fetal bovine serum for 4 hr to attach on plate. For starvation, the cells were pre-incubated in serum-free DMEM and exposed to pro-inflammatory cytokines for 12 hr or TCDD/DMSO for 24 hr. These cells were subjected to qPCR analysis.

Reporter gene assays

Ces3-1.4k and *Ces3*-0.7k promoters were amplified and inserted into pGL4.10 vector (Promega, Fitchburg, WI). Mutation of putative STAT3- and SMAD3-binding sites in the *Ces3*-1.4k reporter vector was produced by PCR mutagenesis with PfuUltra™ HF (Stratagene, La Jolla, CA). The primer sequences are listed in Table S1. The firefly luciferase reporter vectors (200 ng) were transfected into Hepa1c1 cells seeded on 24-well plate, together with pGL4.74 vector (renilla luciferase vector, 10 ng) for normalization. Twelve hours after the transfection, IL6 or TGFβ was added to the cells. Then 24 hours later, the cells were lysed and subjected to measuring the activity with Dual-luciferase assay kit (Promega). The firefly luciferase activity was normalized to the renilla luciferase activity.

In vivo ChIP assays

Mice were injected with 100 μg/kg of TCDD or OIL (10% DMSO/90% corn oil) for control. Four days after injection, the liver tissue was perfused with 2 mg/mL collagenase and fixed at 37 °C with DMEM including 1% formaldehyde and 2 mM disuccinimityl glutarate. ChIP was performed using chromatin immunoprecipitation assay kit (Cell signaling, Irvine, CA) with anti-SMAD3 (ab28379, Abcam, Cambridge, UK) and anti-STAT3 (#9132, Cell signaling) antibodies. The immunoprecipitated DNA was subjected to qPCR. The primer sequences are listed in Table S1. Values were quantified using the comparative CT method and normalized to 2% input, and the data (fold activation) were estimated as ratios to the OIL.

Generation of adenovirus with CES3 expression

The recombinant adenovirus expressing mouse CES3 was prepared by Vector BioLabs, Philadelphia, PA. The virus was amplified in HEK293 cells and purified through 2 rounds of CsCl gradients. The titer was determined by O.D and qPCR. The University of Michigan Vector Core facility provided the control adenovirus expressing green fluorescent protein (GFP) (Ad-GFP). Adenovirus was diluted in 0.9% sterile saline just prior to injection and injected from tail vein with 2×10^9 pfu in the total volume of 200 μL. Mice were sacrificed 4 days after adenovirus injection.

Western blotting

For whole cell extracts, liver was homogenized with RIPA buffer. The homogenate was centrifuged at 18,000*g*. The supernatant was collected and subjected to Western blotting. The samples were boiled for 5 min, loaded in each lane (40 μg of protein), separated in 4–15% gradient gel, and then transferred to PVDF using standard Western blotting techniques. The membranes were incubated with a goat polyclonal antibody against CES3 (sc-82554, Santa Cruz Biotechnology, Santa Cruz, CA).

Histological analysis

Small blocks of liver tissue were immediately fixed in 10% neutral formalin and embedded in paraffin. Sections (4 μm thick) were stained with hematoxylin and eosin. At least 3 discontinuous liver sections were evaluated for each mouse.

Statistical analysis

Statistical analysis was performed using Prism® version 5.0c (GraphPad Software Inc.). A p-value of less than 0.05 was considered as significant difference. Results are expressed as the mean value and SD.

Supplementary Material

Refer to Web version on PubMed Central for supplementary material.

Acknowledgments

This work was supported by the National Cancer Institute Intramural Research Program, Center for Cancer Research. We thank John Buckley and Linda Byrd for technical assistance (National Cancer Institute, NIH). Lalage Wakefield (National Cancer Institute, NIH) provided the SMAD3 expression vector and the SMAD3-binding luciferase vector, Arthur Hurwitz (National Cancer Institute, NIH) provided the STAT3 expression vector and the STAT3-binding luciferase vector, and Shioko Kimura (National Cancer Institute, NIH) furnished the CEBPα expression vector. TM was supported by a fellowship from the Japanese Society for the Promotion of Science.

Abbreviations

AhR	arylhydrocarbon receptor
ARNT	AhR nuclear translocator
ALT	alanine aminotransferase
AST	aspartate aminotransferase
Az	azelaic acid
CEBPα	CCAAT/enhancer binding protein alpha
CES	carboxylesterase
ChIP	chromatin immunoprecipitation
COL1A1	collagen type I alpha 1
CYP	cytochrome P450
GFP	green fluorescent protein
IL	interleukin
iNOS	nitric oxide synthase 2
Km	Michaelis-Menten constant
MCD	methionine- and choline-deficient
MCS	methionine- and choline-supplemented
NASH	nonalcoholic steatohepatitis
NOX2	NADPH oxidase 2
PPIA	peptidylprolyl isomerase A
PCA	principal component analysis

PLS-DA	partial least squares-discriminant analysis
qPCR	quantitative polymerase chain reaction
ROS	reactive oxygen species
SMAD3	MAD homolog 3
SOCS3	suppressor of cytokine signaling 3
STAT3	signal transducer and activator of transcription 3
TCDD	2,3,7,8-tetrachlorodibenzo-p-dioxin
TG	triglyceride
TGFβ	transforming growth factor beta
TGH	triglyceride hydrolase
TNFα	tumor necrosis factor alpha
UPLC-ESI-QTOFMS	ultra-performance liquid chromatography coupled with electrospray ionization quadrupole time-of-flight mass spectrometry
Vmax	maximum enzyme velocity
XDH	xanthine dehydrogenase

References

Fernandez-Salguero P, Pineau T, Hilbert DM, McPhail T, Lee SS, Kimura S, Nebert DW, Rudikoff S, Ward JM, Gonzalez FJ. Immune system impairment and hepatic fibrosis in mice lacking the dioxin-binding Ah receptor. Science. 1995; 268:722–726. [PubMed: 7732381]

Fernandez-Salguero PM, Hilbert DM, Rudikoff S, Ward JM, Gonzalez FJ. Aryl-hydrocarbon receptor-deficient mice are resistant to 2,3,7,8-tetrachlorodibenzo-p-dioxin-induced toxicity. Toxicol Appl Pharmacol. 1996; 140:173–179. [PubMed: 8806883]

Fletcher N, Wahlstrom D, Lundberg R, Nilsson CB, Nilsson KC, Stockling K, Hellmold H, Hakansson H. 2,3,7,8-Tetrachlorodibenzo-p-dioxin (TCDD) alters the mRNA expression of critical genes associated with cholesterol metabolism, bile acid biosynthesis, and bile transport in rat liver: a microarray study. Toxicol Appl Pharmacol. 2005; 207:1–24. [PubMed: 16054898]

Hanlon PR, Zheng W, Ko AY, Jefcoate CR. Identification of novel TCDD-regulated genes by microarray analysis. Toxicol Appl Pharmacol. 2005; 202:215–228. [PubMed: 15667827]

Idle JR, Gonzalez FJ. Metabolomics. Cell Metab. 2007; 6:348–351. [PubMed: 17983580]

Ito S, Chen C, Satoh J, Yim S, Gonzalez FJ. Dietary phytochemicals regulate whole-body CYP1A1 expression through an arylhydrocarbon receptor nuclear translocator-dependent system in gut. J Clin Invest. 2007; 117:1940–1950. [PubMed: 17607366]

Jaeschke H. Reactive oxygen and mechanisms of inflammatory liver injury: Present concepts. J Gastroenterol Hepatol. 2011; 26(Suppl 1):173–179. [PubMed: 21199529]

Johnson CH, Patterson AD, Idle JR, Gonzalez FJ. Xenobiotic Metabolomics: Major Impact on the Metabolome. Annu Rev Pharmacol Toxicol. 2011

Kale RK. Post-irradiation free radical generation: evidence from the conversion of xanthine dehydrogenase into xanthine oxidase. Indian J Exp Biol. 2003; 41:105–111. [PubMed: 15255600]

Lam GY, Huang J, Brumell JH. The many roles of NOX2 NADPH oxidase-derived ROS in immunity. Semin Immunopathol. 2010; 32:415–430. [PubMed: 20803017]

Lin S, Yang Z, Shen Y, Cai Z. LC/MS-based non-targeted metabolomics for the investigation of general toxicity of 2,3,7,8-tetrachlorodibenzo-p-dioxin in C57BL/6J and DBA/2J mice. Int J Mass Spectrom. 2011; 301:29–36.

Lu H, Cui W, Klaassen CD. Nrf2 protects against 2,3,7,8-tetrachlorodibenzo-p-dioxin (TCDD)-induced oxidative injury and steatohepatitis. Toxicol Appl Pharmacol. 2011; 256:122–135. [PubMed: 21846477]

Matsubara T, Tanaka N, Patterson AD, Cho JY, Krausz KW, Gonzalez FJ. Lithocholic acid disrupts phospholipid and sphingolipid homeostasis leading to cholestasis in mice. Hepatology. 2011; 53:1282–1293. [PubMed: 21480330]

Nebert DW, Dalton TP, Okey AB, Gonzalez FJ. Role of aryl hydrocarbon receptor-mediated induction of the CYP1 enzymes in environmental toxicity and cancer. J Biol Chem. 2004; 279:23847–23850. [PubMed: 15028720]

Peters JM, Narotsky MG, Elizondo G, Fernandez-Salguero PM, Gonzalez FJ, Abbott BD. Amelioration of TCDD-induced teratogenesis in aryl hydrocarbon receptor (AhR)-null mice. Toxicol Sci. 1999; 47:86–92. [PubMed: 10048156]

Rifkind AB. CYP1A in TCDD toxicity and in physiology-with particular reference to CYP dependent arachidonic acid metabolism and other endogenous substrates. Drug Metab Rev. 2006; 38:291–335. [PubMed: 16684662]

Shah YM, Matsubara T, Ito S, Yim SH, Gonzalez FJ. Intestinal hypoxia-inducible transcription factors are essential for iron absorption following iron deficiency. Cell Metab. 2009; 9:152–164. [PubMed: 19147412]

Shen ES, Gutman SI, Olson JR. Comparison of 2,3,7,8-tetrachlorodibenzo-p-dioxin-mediated hepatotoxicity in C57BL/6J and DBA/2J mice. J Toxicol Environ Health. 1991; 32:367–381. [PubMed: 2016751]

Sugihara K, Kitamura S, Yamada T, Ohta S, Yamashita K, Yasuda M, Fujii-Kuriyama Y. Aryl hydrocarbon receptor (AhR)-mediated induction of xanthine oxidase/xanthine dehydrogenase activity by 2,3,7,8-tetrachlorodibenzo-p-dioxin. Biochem Biophys Res Commun. 2001; 281:1093–1099. [PubMed: 11243847]

Tanaka N, Matsubara T, Krausz KW, Patterson AD, Gonzalez FJ. Disruption of phospholipid and bile acid homeostasis in mice with nonalcoholic steatohepatitis. Hepatology. 2012; 56:118–129. [PubMed: 22290395]

Thomae TL, Glover E, Bradfield CA. A maternal Ahr null genotype sensitizes embryos to chemical teratogenesis. J Biol Chem. 2004; 279:30189–30194. [PubMed: 15145931]

Thurmond TS, Staples JE, Silverstone AE, Gasiewicz TA. The aryl hydrocarbon receptor has a role in the in vivo maturation of murine bone marrow B lymphocytes and their response to 2,3,7,8-tetrachlorodibenzo-p-dioxin. Toxicol Appl Pharmacol. 2000; 165:227–236. [PubMed: 10860871]

Tomita S, Sinal CJ, Yim SH, Gonzalez FJ. Conditional disruption of the aryl hydrocarbon receptor nuclear translocator (Arnt) gene leads to loss of target gene induction by the aryl hydrocarbon receptor and hypoxia-inducible factor 1alpha. Mol Endocrinol. 2000; 14:1674–1681. [PubMed: 11043581]

Vorderstrasse BA, Steppan LB, Silverstone AE, Kerkvliet NI. Aryl hydrocarbon receptor-deficient mice generate normal immune responses to model antigens and are resistant to TCDD-induced immune suppression. Toxicol Appl Pharmacol. 2001; 171:157–164. [PubMed: 11243915]

Yamamoto T, Matsuda T, Muraguchi A, Miyazono K, Kawabata M. Cross-talk between IL-6 and TGF-beta signaling in hepatoma cells. FEBS Lett. 2001; 492:247–253. [PubMed: 11257503]

Yang D, Li Y, Yuan X, Matoney L, Yan B. Regulation of rat carboxylesterase expression by 2,3,7,8-tetrachlorodibenzo-p-dioxin (TCDD): a dose-dependent decrease in mRNA levels but a biphasic change in protein levels and activity. Toxicol Sci. 2001; 64:20–27. [PubMed: 11606798]

- Dioxin altered hepatic CES3 resulting in elevated serum azelaic acid-mono esters.
- Decreased CES3 expression is due to pro-inflammatory cascade activation.
- The CES3-mediated metabolic changes are associated with steatohepatitis.
- Azelaic acid-mono ester is an indicator of dioxin exposure and steatohepatitis.

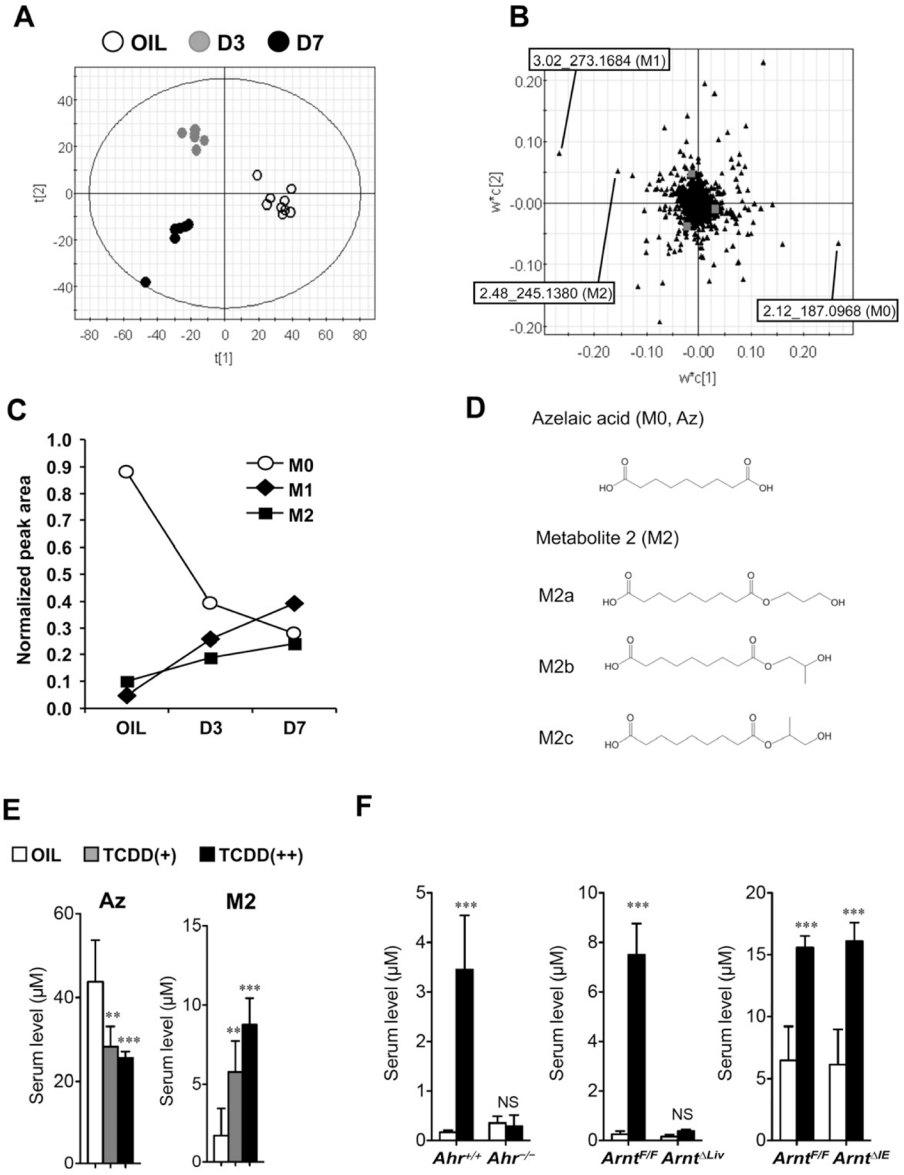

Figure 1. Identification of serum metabolites altered by TCDD exposure

(A) PLS-DA of the serum metabolites between OIL (vehicle, opened circle) and TCDD [3 days later (D3), gray-closed circle; 7 days later (D7), black-closed circle].

(B) Loading plot of the PLS-DA.

(C) Time course of serum TCDD markers (M0, M1, and M2) after exposure to 200 μg/kg TCDD. Amounts were normalized to the additional 4-chloropropamide. Data represent the mean (n=5–9).

(D) Chemical structures of identified TCDD markers (M0 and M2).

(E) Quantification of azelaic acid (Az) and M2 levels in serum (C57BL/6) after TCDD exposure. Each bar represents the mean value and SD (n=4–9).

(F) Serum M2 levels in *Ahr*$^{-/-}$, *Arnt*$^{\Delta Liv}$ and *Arnt*$^{\Delta IE}$ mice. Each bar represents the mean value and SD (n=3–9). Significance was determined by one-way ANOVA with Dunnett's test (E) or Bonferroni's test (F). *, P<0.05; **, P<0.01; ***, P<0.001; NS, no significance.

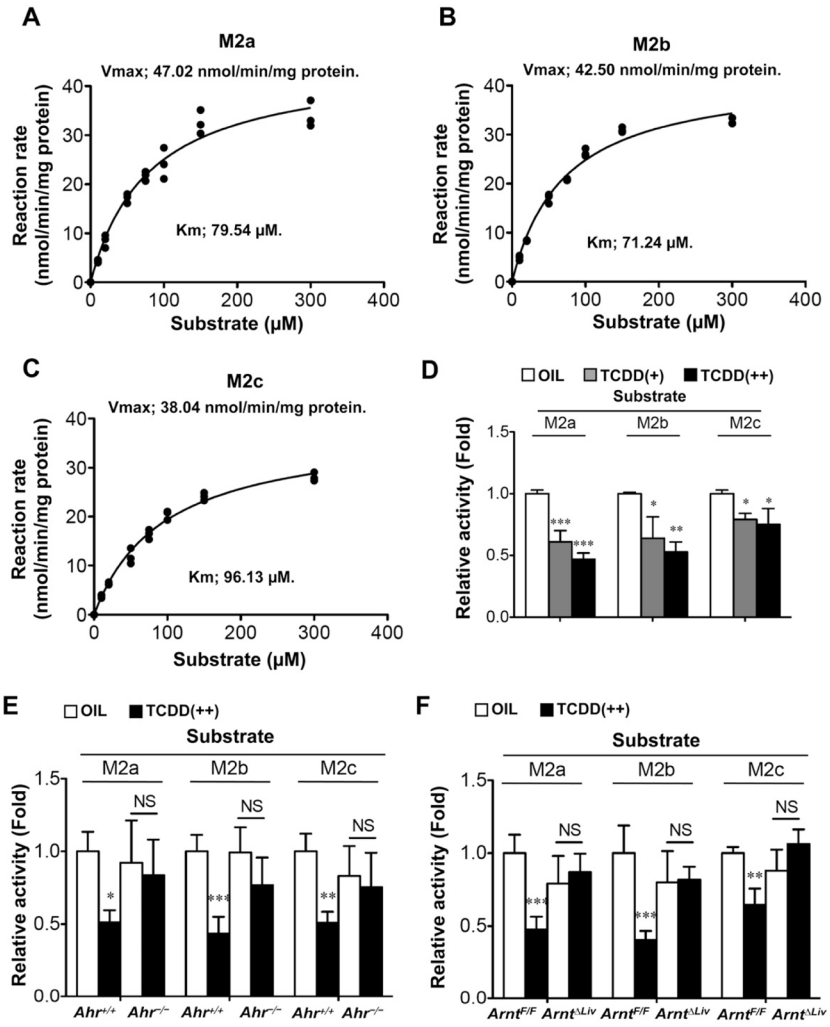

Figure 2. TCDD exposure lowered microsomal M2 hydrolysis activities in the livers

(A–C) Kinetic analysis of microsomal M2 in liver of male C57BL/6 mouse (A, M2a; B, M2b; C, M2c). Hydrolase activity, Vmax, and Km were estimated as described in Experimental Procedures.

(D–F) Changes in hepatic microsomal activity of M2 hydrolysis after TCDD injection (D, C57BL/6, E, *Ahr*$^{-/-}$; F, *Arnt*$^{\Delta Liv}$). Value was expressed as ratio to the wild-type mice treated with OIL. Each bar represents the mean value and SD (n=3–5). Significance was determined by one-way ANOVA with Dunnett's test (D) or Bonferroni's test (E and F). *, P<0.05; **, P<0.01; ***, P<0.001; NS, no significance.

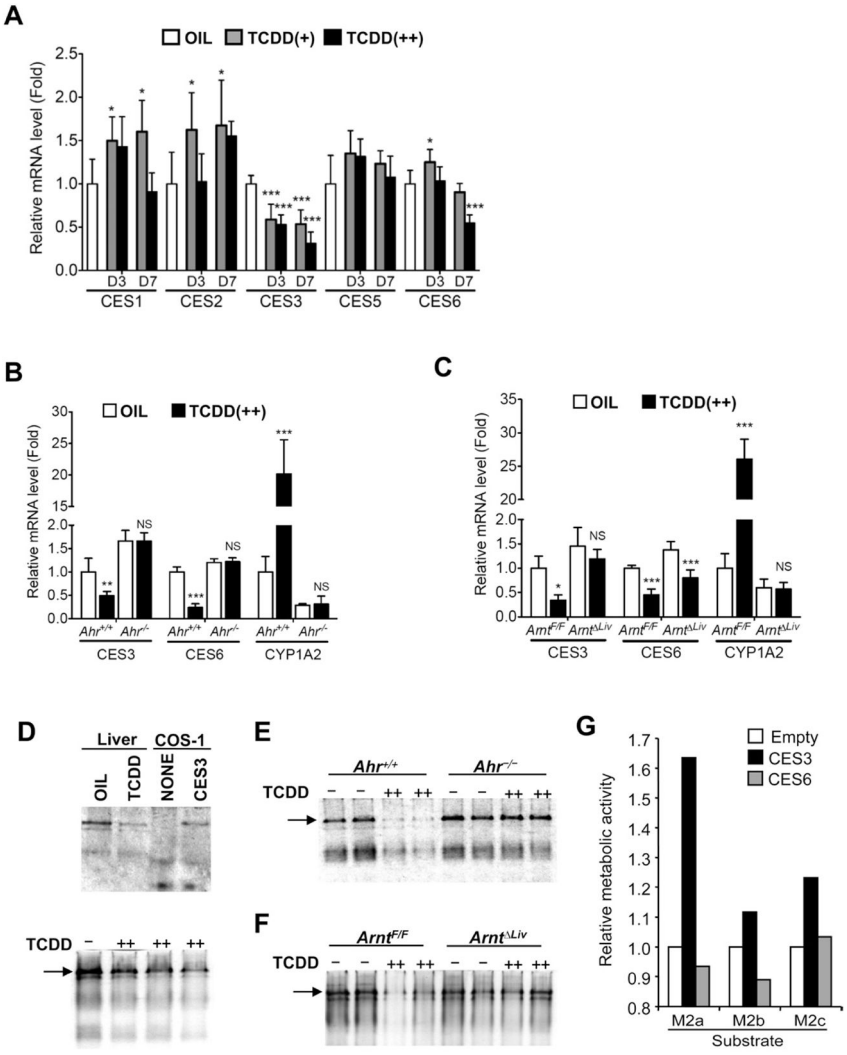

Figure 3. TCDD exposure decreased carboxylesterase 3 levels in the livers, which mediated M2 hydrolysis

(A–C) qPCR analysis of CES mRNAs in the livers (A, C57BL/6; B, *Ahr*$^{-/-}$; C, *Arnt*$^{\Delta Liv}$). Expression was normalized to 18S ribosomal RNA. Each bar represents the mean value and SD (n=4–5). OIL, TCDD(+) and TCDD(++) denotes vehicle, 10, and 200 μg/kg TCDD, respectively. D3 and D7 indicate 3 days and 7 days after TCDD injection, respectively. Significance was determined by one-way ANOVA with Dunnett's test (A) or Bonferroni's test (B and C). *, P<0.05; **, P<0.01; ***, P<0.001; NS, no significance.

(D–F) Non-denaturing gel electrophoresis of the liver microsomal fraction (D, C57BL/6; E, *Ahr*$^{-/-}$; F, *Arnt*$^{\Delta Liv}$). Non-denaturing gel electrophoresis and CES staining were performed as described in Experimental Procedures. Arrows indicate CES3 proteins. (G) M2 hydrolase activity of cells transformed with CES3. The hydrolase activity of cells was estimated as described in Experimental Procedures. Hepa1c1 cells were transfected with empty, CES3-expression, and CES6-expression vectors, respectively.

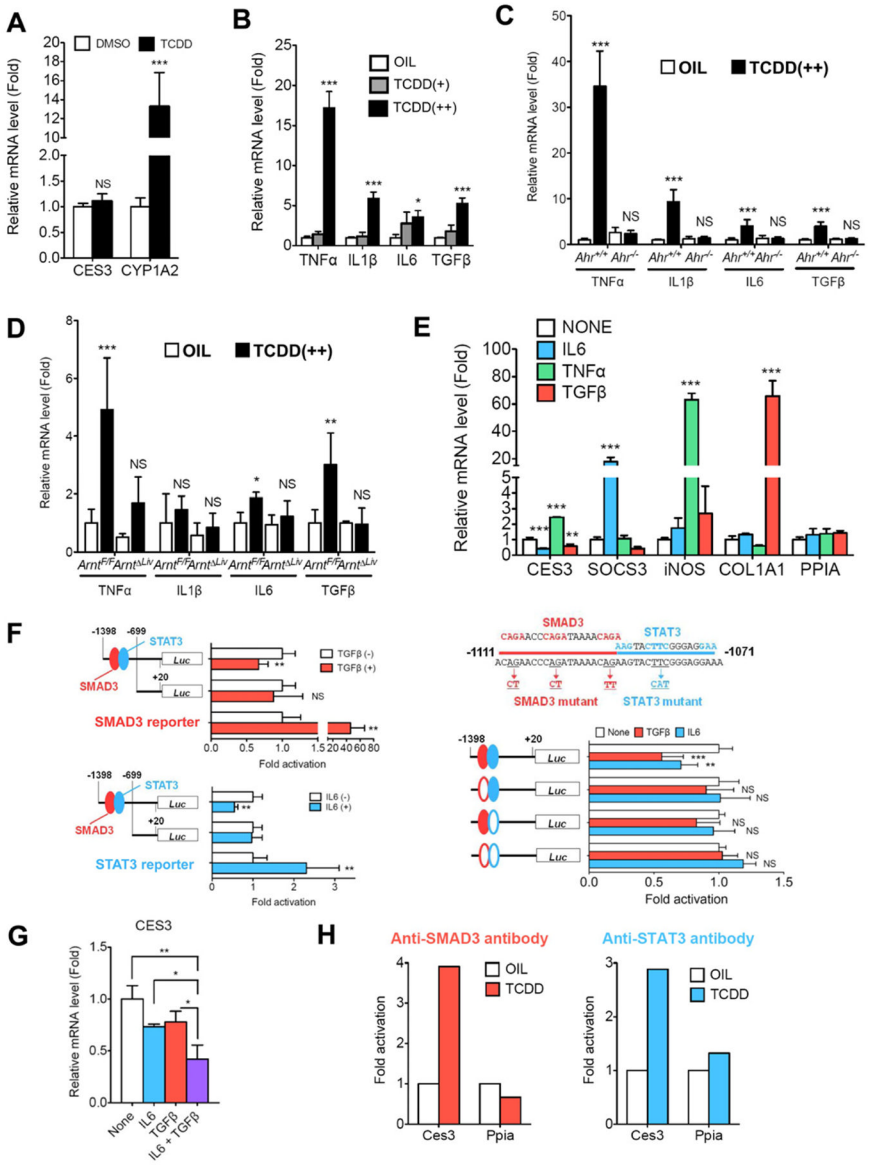

Figure 4. TCDD-stimulated activation of IL6 and TGFβ signals attenuated *Ces3* gene transcription in the livers

(A) CES3 and CYP1A2 mRNA levels in primary hepatocyte after TCDD exposure. Each bar represents the mean value and SD (n=4).

(B–D) qPCR analysis of pro-inflammatory cytokine mRNAs in the livers (B, C57BL/6; C, *Ahr*$^{-/-}$; D, *Arnt*$^{\Delta Liv}$). Each bar represents the mean value and SD (n=4–5).

(E) CES3 mRNA in primary hepatocyte after exposure to pro-inflammatory cytokine (100 ng/mL of IL6, 100 ng/mL of TNFα or 10 ng/mL of TGFβ). Each bar represents the mean value and SD (n=3). SOCS3, iNOS and COL1A1 mRNA expression was used as positive controls for IL6, TNFα, and TGFβ, respectively.

(F) *Ces3* gene promoter assay. Each bar represents the mean value and SD (n=6). IL6 (100 ng/mL) or TGFβ (5 ng/mL) was added to the Hepa1c1 cells transfected with the reporter vectors. Significance was determined by unpaired t-test (left) and one-way ANOVA with Dunnett's test (right).

(G) CES3 mRNA in primary hepatocyte after co-exposure to pro-inflammatory cytokine (50 ng/mL of IL6 and 5 ng/mL of TGFβ). Each bar represents the mean value and SD (n=3). Significance was determined by one-way ANOVA with Bonferroni's test.
(H) *In vivo* ChIP assays. Each bar represents the average value (n=2). The *Ppia* gene was used as negative target gene of STAT3 and SMAD3.

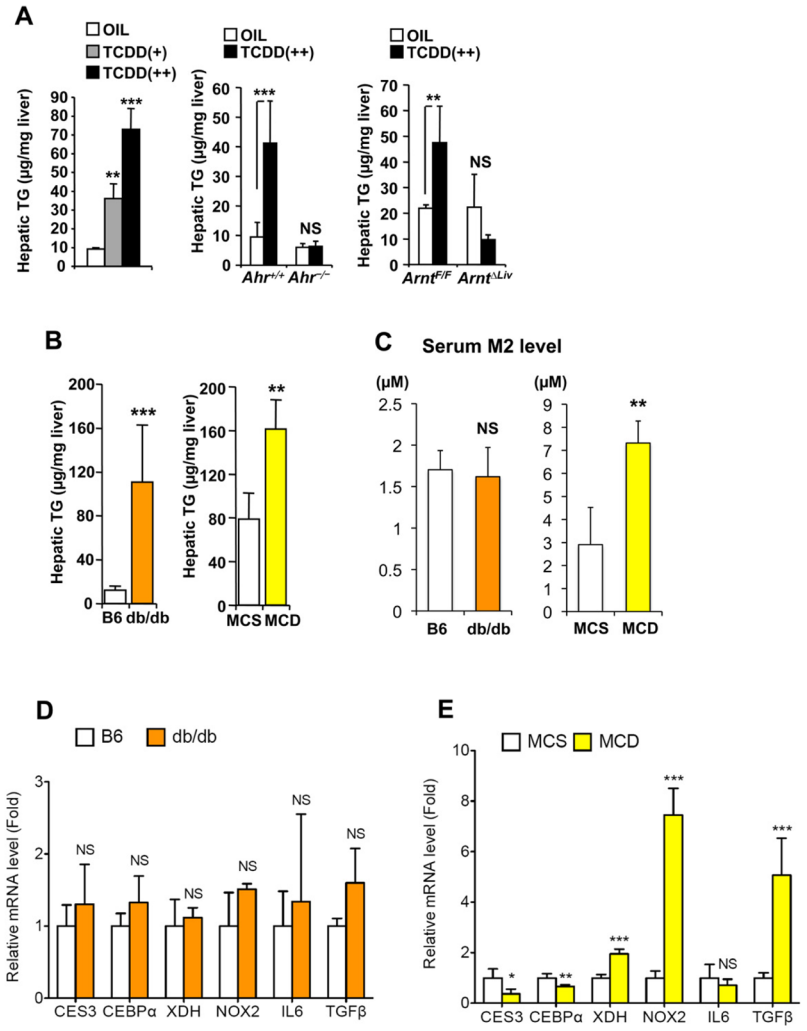

Figure 5. TCDD-induced hepatic alterations in Az-mono ester metabolism were also detected in other steatohepatitis model, but not simple steatosis model

(A–B) Hepatic TG levels in C57BL/6 (A), *db/db* and MCD diet-treated mice (B). Oil, TCDD(+) and TCDD(++) denote vehicle, 10 and 200 μg/kg TCDD, respectively. Significance was determined by one-way ANOVA with Dunnett's test (C57BL/6) or Bonferroni's test ($Ahr^{-/-}$ and $Arnt^{\Delta Liv}$) and unpaired t-test (*db/db* and MCD). Each bar represents the mean value and SD (n=3–6). **, P<0.01; ***, P<0.001; NS, no significance. (C–E) Serum M2 levels (C) and qPCR analysis of hepatic TCDD-related gene expression in *db/db* (D) and MCD diet-treated mice (E). Significance was determined by unpaired t-test. Each bar represents the mean value and SD (n=3–6). *, P<0.05; **, P<0.01; ***, P<0.001; NS, no significance.

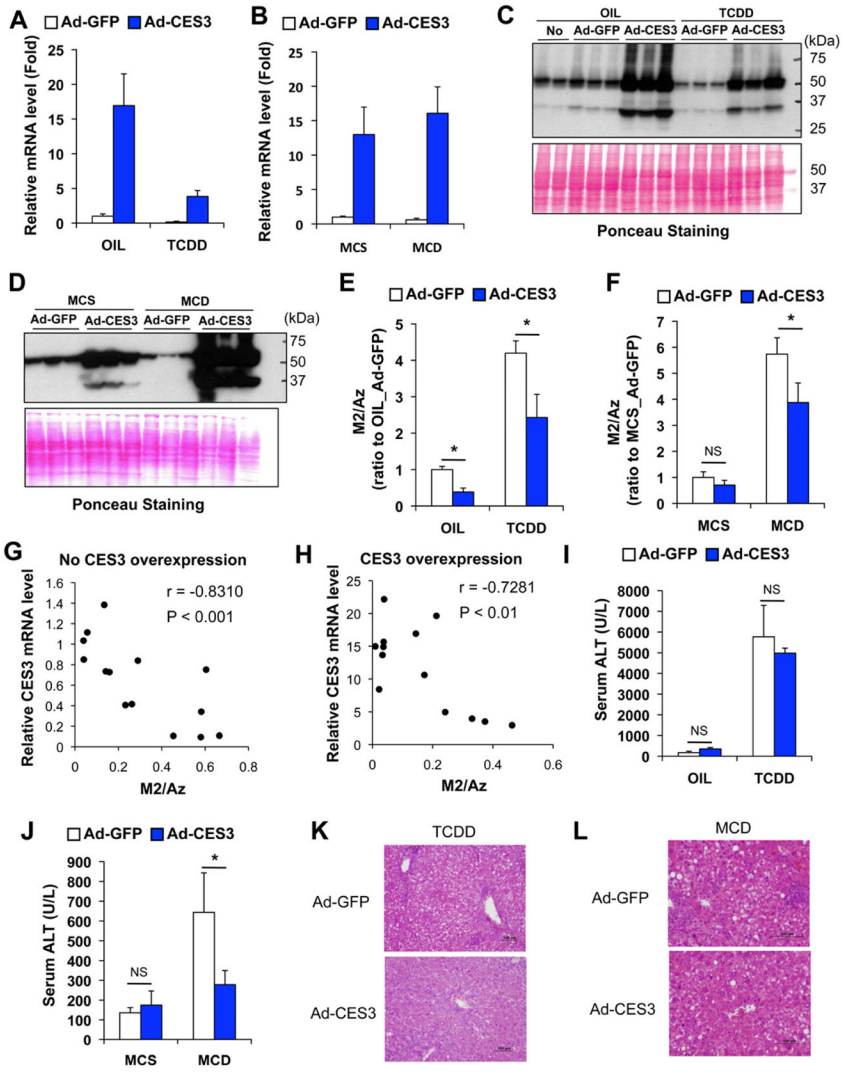

Figure 6. Introduction of hepatic CES3 expression with adenovirus attenuated TCDD- and MCD-induced hepatic alterations in Az-mono ester metabolism

(A–B) Hepatic CES3 mRNA levels after injection of adenovirus expressing mouse CES3 (Ad-CES3) or control adenovirus (Ad-GFP) under condition of TCDD (A)- and MCD diet (B)-induced liver injury. Expression was normalized to 18S ribosomal RNA. Each bar represents the mean value and SD (n=3–4). OIL, TCDD, MCS and MCD denote vehicle, 200 μg/kg TCDD, methionine- and choline-supplemented diet, and methionine- and choline-deficient diet, respectively.

(C–D) Western blotting of hepatic CES3 protein after injecting Ad-CES3 and Ad-GFP to mice treated with TCDD (C) and MCD diet (D).

(E–F) Serum M2/Az ratios after injecting Ad-CES3 and Ad-GFP to mice treated with TCDD (E) and MCD diet (F). The value was presented as fold to OIL_Ad-GFP (E) or MCS_Ad-GFP (F). Each bar represents the mean value and SD (n=3–4). Significance was determined by one way-ANOVA with Bonferroni's test. *, P<0.05; NS, no significance.

(G–H) Correlation between hepatic CES3 mRNA levels and serum M2/Az ratios under condition without (G) and with CES3 overexpression (H). The correlation r and p values were estimated by Pearson correlation test.

(I–J) Serum ALT levels after injecting Ad-CES3 and Ad-GFP to mice treated with TCDD (I) and MCD diet (J). Each bar represents the mean value and SD (n=3–4). Significance was determined by one-way ANOVA with Bonferroni's test. *, P<0.05; NS, no significance. (K–L) Liver histology with hematoxylin and eosin staining. Bars represent 100 μm.

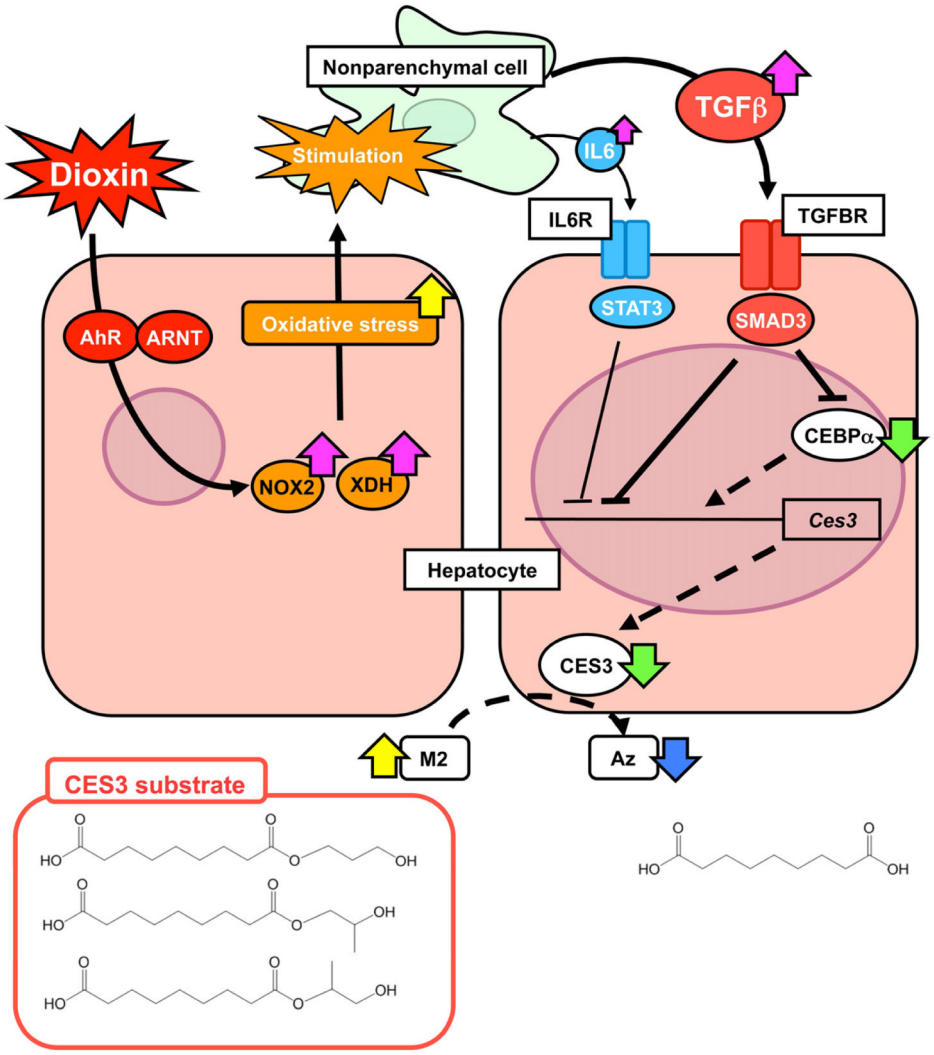

Figure 7. Putative mechanism by which dioxin mediates hepatic alterations in M2 metabolism

Yellow and blue arrow represents increased and decreased chemical, respectively. Pink and green arrow is presented as enhanced and attenuated gene expression, respectively. Bold and broken line denotes acceleration and deceleration, respectively.